*J. Fluid Mech.* (1995), *vol.* 294, *pp.* 259–281



# Stability of the viscous flow of a fluid through a flexible tube

By V. KUMARAN

Department of Chemical Engineering, Indian Institute of Science, Bangalore 560 012, India

(Received 8 April 1994 and in revised form 18 January 1995)

The stability of Hagen–Poiseuille flow of a Newtonian fluid of viscosity $\eta$ in a tube of radius $R$ surrounded by a viscoelastic medium of elasticity $G$ and viscosity $\eta_s$ occupying the annulus $R < r < HR$ is determined using a linear stability analysis. The inertia of the fluid and the medium are neglected, and the mass and momentum conservation equations for the fluid and wall are linear. The only coupling between the mean flow and fluctuations enters via an additional term in the boundary condition for the tangential velocity at the interface, due to the discontinuity in the strain rate in the mean flow at the surface. This additional term is responsible for destabilizing the surface when the mean velocity increases beyond a transition value, and the physical mechanism driving the instability is the transfer of energy from the mean flow to the fluctuations due to the work done by the mean flow at the interface.

The transition velocity $\Gamma_t$ for the presence of surface instabilities depends on the wavenumber $k$ and three dimensionless parameters: the ratio of the solid and fluid viscosities $\eta_r = (\eta_s/\eta)$, the capillary number $\Lambda = (T/GR)$ and the ratio of radii $H$, where $T$ is the surface tension of the interface. For $\eta_r = 0$ and $\Lambda = 0$, the transition velocity $\Gamma_t$ diverges in the limits $k \ll 1$ and $k \gg 1$, and has a minimum for finite $k$. The qualitative behaviour of the transition velocity is the same for $\Lambda > 0$ and $\eta_r = 0$, though there is an increase in $\Gamma_t$ in the limit $k \gg 1$. When the viscosity of the surface is non-zero ($\eta_r > 0$), however, there is a qualitative change in the $\Gamma_t$ *vs.* $k$ curves. For $\eta_r < 1$, the transition velocity $\Gamma_t$ is finite only when $k$ is greater than a minimum value $k_{min}$, while perturbations with wavenumber $k < k_{min}$ are stable even for $\Gamma \to \infty$. For $\eta_r > 1$, $\Gamma_t$ is finite only for $k_{min} < k < k_{max}$, while perturbations with wavenumber $k < k_{min}$ or $k > k_{max}$ are stable in the limit $\Gamma \to \infty$. As $H$ decreases or $\eta_r$ increases, the difference $k_{max} - k_{min}$ decreases. At a minimum value $H = H_{min}$ which is a function of $\eta_r$, the difference $k_{max} - k_{min} = 0$, and for $H < H_{min}$, perturbations of all wavenumbers are stable even in the limit $\Gamma \to \infty$. The calculations indicate that $H_{min}$ shows a strong divergence proportional to $\exp(0.0832\eta_r^2)$ for $\eta_r \gg 1$.

## 1. Introduction

The stability of fluid flow near a flexible surface is of interest in diverse applications such as marine and aerospace propulsion, biotechnology and polymer processing applications. The flow of a fluid through a tube with flexible walls is observed in biological systems in the transport of blood and other biological fluids, as well as in biotechnology applications which involve flows past polymer matrices and membranes. There has not been much systemmatic work done on the flow of fluid through flexible tubes such as blood vessels in biological systems. It is usually assumed that the flow characteristics are the same as those of the flow through a rigid tube, where there is a

laminar-to-turbulent transition at Reynolds numbers between 2100 and 4000 due to the fluid inertia. However, the experiments of Krindel & Silberberg (1979) (discussed a little later), suggest that the stability characteristics of this flow could be very different from those of the flow in a tube with rigid walls. In particular, an anomalous drag force is observed when the fluid velocity is increased beyond a critical value which depends on the fluid viscosity and the wall elasticity, in addition to the dimensions of the tube and wall. The nature of the instability observed is also different: in a flexible tube, there is a gradual increase in the drag force as the Reynolds number is increased, in contrast to the sharp (almost discontinuous) jump in the drag force in a rigid tube at the critical Reynolds number.

Krindel & Silberberg propose a correlation for the critical velocity which is independent of the fluid density, suggesting that the instability is not driven by inertial forces. This is rather surprising, because the instability in the flow in a rigid tube is due to inertial effects, and fluid flows are usually stable in the absence of inertia. To test the possibility of a non-inertial destabilizing mechanism, a simple model of a Newtonian fluid flowing through a tube with a flexible wall is analysed in this paper. A linear stability analysis is used to examine a possible destabilizing mechanism, and to determine the parameter ranges where the instability might be expected. From a technological viewpoint, the presence of an instability has two effects: it increases the drag force and the power consumption, and it also enhances mixing and heat and mass transfer. In processes where it is advantageous to have lower drag forces, the wall and fluid properties could be adjusted so that the flow is stable and remains in the laminar regime. Alternatively, in situations where greater mixing and heat or mass transfer are desirable, the fluid and wall properties could be suitably chosen to make the flow unstable. Therefore, a detailed examination of the mechanism responsible for destabilizing the flow could be of use in biotechnology applications. In this introduction, previous studies in related areas are briefly summarized and a few representative papers are cited in each area, and then the objective of the present work is discussed.

The study of high Reynolds number flow of a fluid past a compliant surface has been motivated by the desirability of drag reduction in marine and aerospace propulsion. Kramer (1957, 1960) first suggested, based on his experiments on flow past compliant coatings, that the flexibility of the surface could reduce the turbulent drag. The effect of a flexible boundary on hydrodynamic stability were first studied by Benjamin (1960, 1963) and Landahl (1962). By a simple extension of the conventional stability theory of Tollmien (1929) and Schlichting (1933), Benjamin (1960) showed that a flexible non-dissipative wall tends to stabilize the Tollmien–Schlichting instability, which is the destabilizing mechanism in the flow past a rigid surface. In addition, Benjamin and Landahl pointed out that there is an additional mode of instability that could exist in an inviscid flow, which was termed the flow-induced surface instability. Since then, there has been much work on the flow past a Kramer-type surface (see, for example Carpenter & Garrad (1985, 1986), Carpenter & Gajjar (1990) and the review article by Carpenter (1990) and the references therein). Most of the subsequent studies have determined the stability by a numerical solution of the Orr–Sommerfeld equation for the fluid velocity, which requires sophisticated numerical techniques due to the stiffness of the governing equation. An asymptotic analysis was used by Carpenter & Gajjar (1990) to obtain the stability characteristics when the critical layer near the wall is well separated from the viscous sublayer, and Carpenter & Garrad (1986) used a potential flow calculation to derive approximate stability criteria. The consensus appears to be that a compliant wall does indeed lead to drag reduction owing to a

postponement in the transition from laminar to turbulent flow. A numerical study of the effect of flexible walls on the stability of plane Poiseuille flow was carried out by Green & Ellen (1972), using an extension of the techniques developed by Lin (1945*a–c*, 1955). However, there does not appear to be much work on the flow through a tube bounded by a flexible wall. In part, this may be because the flow through a rigid tube is always stable within the linear theory, and the Tollmien–Schlichting instability does not exist for a rigid tube.

The collapse of a flexible tube due to the difference between the internal and external pressures has also been extensively studied. Some fairly detailed experiments were conducted by Bertram (1986, 1987) where many types of oscillatory behaviour were observed at different values of the flow rate and difference between external and internal pressure, and these transitions have subsequently been characterized (see Bertram, Raymond & Pedley 1989). This problem has also been studied theoretically by Cancelli & Pedley (1985), Reyn (1987), Jensen & Pedley (1989) and others. In the theoretical studies, the cross-sectional area of the tube is related to the difference between the external and internal pressure, with an additional term to account for the effect of longitudinal tension. The flow in the tube is in the turbulent regime, and so the energy dissipation is neglected. The mass, momentum and energy balance equations are solved to determine the variation in the cross-sectional area and pressure as a function of the difference between the external and outlet pressure and the flow rate. Jensen & Pedley (1989) report reasonable agreement between theoretical predictions and experimental observations despite some simplifications made in the theoretical treatment.

The studies discussed above consider the stability at high Reynolds number, where the fluid inertia plays an important role in destabilizing the flow. However, the inertial effects are absent in a low Reynolds number flow, and instabilities have to be driven by a different mechanism in this case. The low Reynolds number flow of a Newtonian fluid past a rigid surface is always stable because the Stokes equations are not explicitly dependent on time, but the flow of viscoelastic liquids could become unstable due to the time dependence of the elastic terms in the momentum equations. The stability of the flow of a viscoelastic fluid down an inclined plane was studied using a long-wavelength analysis by Gupta (1967), and subsequently extended to finite wavelengths by Shaqfeh, Larson & Fredrickson (1989). These studies found that the critical Reynolds number for the onset of surface instabilities is lowered by viscoelastic effects, but the fluid inertia is still necessary to destabilize the flow. Yih (1970) used a long-wavelength analysis to show that the interface between two fluids of different viscosities can become unstable when the difference in strain rate increases beyond a critical value even at low Reynolds number. Hooper & Boyd (1983) found a similar instability for short waves. Waters & Keely (1987) used a long-wavelength analysis to examine the stability between two viscoelastic liquids, and found that there are unstable modes only when the viscosities of the two fluids are different. Renardy (1988) predicted, based on a finite-wavelength analysis, that there could be an instability even when the viscosities are equal. All the above studies require the inclusion of the inertial terms in the conservation equation to predict instabilities.

The instability of the interface between two polymer melts during co-extrusion was studied by Chen (1991) and Su & Khomami (1992). Chen (1991) showed, based on a long-wavelength analysis, that the flow could become unstable due to a discontinuity in the normal stress difference across the interface in the base state. Su & Khomami (1992) studied the flow of viscoelastic fluids through both plane and converging channels. They determined the behaviour in the long-wavelength limit using an

asymptotic analysis and extended the solution to finite wavelengths using analytic continuity. The above-mentioned instabilities due to the discontinuity in the normal stress difference could exist even in the absence of fluid inertia. The stability of the plane Couette flow of a Newtonian fluid adjacent to an elastic gel was studied by Kumaran, Fredrickson & Pincus (1994). Here, the authors found that unstable fluctuations are possible even when the inertia of the fluid and the gel are neglected. The flow is destabilized by the transport of energy from the mean flow to the fluctuations due to a discontinuity in the velocity gradient at the interface.

Experimental work on the flow of a Newtonian fluid through a gel-walled tube was conducted by Krindel & Silberberg (1979). They observed that there is an anomalous increase in the drag force when the fluid velocity is increased beyond a critical value, which they attributed to wall oscillations caused by an instability in the flow. The transition Reynolds number in this system was found to be much lower than the transition Reynolds number $Re = (2\rho \bar{V}_t R/\eta) = 2100$ for the flow through a rigid tube. Here, $\bar{V}_t$ is the transition velocity, $R$ is the radius of the tube, and $\rho$ and $\eta$ are the density and viscosity of the fluid. Krindel & Silberberg used two methods for characterizing the transition to a turbulent flow: visual observation by injecting a dye stream into the center of the tube and drag measurements. In some cases the transition Reynolds number was found to be as low as 570 using the visual observation technique, but the drag measurements indicated that the transition could take place at an even lower velocity. Further, there was found to be a gradual increase in the drag force, in contrast to the near discontinuous jump at the transition Reynolds number in a rigid tube, indicating that the destabilizing mechanism could be different in the present case. The authors obtained the correlation $\bar{V}_t \propto (GR^2/\eta H)$, where $G$ is the shear modulus of the gel and $H$ is the radius of the outer gel wall. The absence of the fluid density in this correlation suggests that fluid inertia may not be important in destabilizing the flow, and the dominant stresses are the viscous stress in the fluid and the elastic stress in the gel. This is very different from a rigid tube, where the inertial stresses destabilize the flow when the Reynolds number is increased beyond the transition value.

In the present paper, a linear analysis is used to determine the stability of a viscous flow in a tube with viscoelastic walls, and to examine the mechanism that could cause unstable oscillations in the wall. The inertia of the fluid and the wall material are neglected in the calculation, and it is useful to examine the parameter ranges where this approximation is valid. The subsequent calculation shows that the inertia can be neglected when the dimensionless number $(Re/\Gamma) \equiv (\rho G R^2/\eta^2) \ll 1$. The shear modulus of elasticity $G$ varies in the range of 10–100 N m$^{-2}$, the lower value being typically encountered in soft biological tissues while the higher limit is applicable to dense polymer gels. The viscosity of fluids and biological suspensions is typically in the range $10^{-2}$–$10^{-3}$ N s m$^{-2}$, while the density of most liquids is about $10^3$ kg m$^{-3}$. For these parameter values, the fluid inertia can be neglected for $R \ll$ (10–100 μm). The surface tension at the interface between the solid and the fluid will be comparable to the elastic stress for capillary number $\Lambda \equiv (T/GR) = O(1)$, where $T$ is the surface tension. The surface tension for a polymer gel is $O(10^{-2}$ N m$^{-1})$, and the stress due to surface tension will be of the same magnitude as the elastic stress for tubes of thickness 100 μm. Tubes of this size are present in the microcirculation system, but there does not appear to be any experimental work that has probed this regime. Krindel & Silberberg (1979) considered a tube of diameter 150 μm, but the coefficient of elasticity of the gel used by them was 100 N m$^{-2}$ and so the parameter $(Re/\Gamma)$ was about 150. However, as mentioned earlier, the experimental correlation derived by them indicated that there is a balance between the viscous stresses in the fluid and the elastic stresses in the wall

at the transition velocity where the flow becomes unstable. This analysis attempts to examine a possible non-inertial mechanism that could drive the instability.

A normal mode analysis is used for determining the stability of the perturbations in this paper. Here, perturbations in the form of Fourier modes are imposed on the base flow, and their temporal growth rate is determined. This method has been used for the classical problems in hydrodynamic stability such as the Rayleigh–Taylor, Kelvin–Helmholtz and Taylor–Couette problems. In the study of the stability of inviscid shear flows, the initial value method is also used, where a disturbance in the form of a localized wave packet in space is imposed on the mean flow, and the spatial growth rate of the perturbations is determined. The relationship between the two techniques is given in Chapter 6 of Drazin & Reid (1981). When the perturbations are neutrally stable, the spatial and temporal modes coincide because both the spatial and temporal growth rates are imaginary. Near the neutral stability curve, the group velocity of the most unstable mode in the temporal description is related to the derivative of the frequency with respect to the wavenumber in the spatial description. Therefore, the normal mode analysis provides direct access to the neutral stability curve, which is our primary interest in the present study, and also to the group velocity of the weakly unstable spatial modes. The normal mode problem is simpler than the initial value problem, and it is possible to obtain analytical results for the growth rate in the former case, whereas the latter involves extensive computation. Consequently, the normal mode analysis is preferred in the present study.

The equations of motion are solved analytically, and the growth rate is determined as a function of the wavenumber, fluid velocity and the wall and fluid properties. This is more advantageous than the easier numerical approach, which involves asymptotic solutions in the long-wavelength limit and extension of the solutions to finite wavelengths, because it turns out that there are certain solutions which cannot be determined from the long-wavelength analysis; this will be discussed further in the conclusions. A detailed understanding of the asymptotic solutions in this limit could be used as a starting point to probe the stability of finite Reynolds number flows, where it is necessary to solve the equations numerically. A continuation procedure starting from the viscous limit may be more reliable than a continuation from the small-wavenumber limit in the present case due to the existence of solutions that are unstable at finite wavenumber but stable in the limit of small wavenumber. The instability will be modified by inertial effects at finite Reynolds number, but the destabilizing mechanism is likely to persist even at finite Reynolds number, whereas the inertial instability becomes operative only at a Reynolds number between 2300 and 4000.

The configuration consists of the flow of a Newtonian fluid in a tube of radius $R$ surrounded by a flexible material at rest in the annular region $R < r < HR$. The motion of the fluid is governed by the Stokes equations, and the inertia of the fluid and the wall are neglected. The dynamics of the wall is governed by a constitutive equation for an incompressible elastic solid (Landau & Lifshitz 1989) modified to include viscous dissipation. This equation has been used previously for polymer gels (see, for example, Harden, Pleiner & Pincus (1991) and Kumaran 1993). The radius of the tube is assumed to be invariant along the axial direction. This approximation is applicable to an incompressible flexible medium in a tube of infinite length. In tubes of finite length, there is a variation in the radius due to the pressure gradient along the tube, and the lengthscale for this variation is the total length of the tube. For example, if the variation in the tube radius is $O(\Delta R)$ over the length of the tube $L$, the slope of the walls is $O(\Delta R/L)$, and the constant-radius approximation is valid for $(\Delta R/L) \ll 1$. In the experiments of Krindel & Silberberg (1979) the radius and length of the tube were

0.075 mm and 4 cm respectively. The variation in the radius of the tube was found to be about 20% of the tube radius, and for this variation the slope of the tube wall is about $7.5 \times 10^{-4}$. In the present analysis fluctuations with wavelength comparable to the tube radius are considered, and the results will be accurate if the variation over a distance comparable to the tube radius is small. The validity of this approximation is supported by the experimental observations of Krindel & Silberberg, who find that the variation is not large enough to explain the anomalous increase in the drag force.

In the unperturbed state, there is a balance between the viscous stresses in the fluid and the elastic stresses in the wall. There is no coupling between the mean flow and the fluctuations in the momentum equation, since the fluid inertia has been neglected. But there is an additional term in the boundary condition for the tangential velocity due to the discontinuity in the strain rate at the surface. This is the only coupling between the mean flow and the perturbations, and is responsible for inducing the instability discussed in this paper. This term, which is proportional to the viscous shear stress in the fluid at the interface, has been incorporated in earlier studies (since Benjamin 1960) of the flow past a flexible surface at high Reynolds number. However, in those studies, this only modifies the existing instabilities because the viscous effects are small at high Reynolds number. In the present case, however, the viscous effects are dominant and the presence of this term completely changes the nature of the flow.

The effects of surface tension and the ratio of the viscosities of the solid and fluid on the critical velocity are examined, and empirical relations are developed for the critical velocity in different limits. The equations of motion are derived in the next section, and the results of the stability analysis are discussed in §3. A brief summary of the important conclusions is given in §4.

## 2. Problem formulation

The system consists of a Newtonian fluid of viscosity $\eta$ flowing in an infinitely long tube of radius $R$, which is surrounded by an incompressible flexible medium having a elastic shear modulus $G$ and a viscosity $\eta_s$ that occupies an annulus of radius $R < r < HR$, as shown in figure 1. The outer wall of the viscoelastic material is fixed to a rigid tube at $r = H$. The base flow in the tube is a pressure-driven Hagen–Poiseuille flow:

$$\bar{v}(r) = \frac{-\mathrm{d}_x p_0}{4\eta}(R^2 - r^2), \tag{2.1}$$

where $\mathrm{d}_x p_0$ is the pressure gradient along the tube. The flexible medium is at rest in the base state, but there is a strain due to the fluid stress at the surface. The momentum conservation equation for the unidirectional displacement field at steady state can be easily solved to obtain

$$\bar{u}_r = \frac{-\mathrm{d}_x p_0}{4G}(H^2 R^2 - r^2). \tag{2.2}$$

Note that the zero displacement boundary conditions at $r = HR$ are satisfied by the above displacement field. In addition, the viscous shear stress due to the strain rate in the fluid is exactly balanced by the elastic stress due to the strain in the surface. As mentioned in the introduction, we consider the limit of low Reynolds number, where the inertia of the fluid and the wall material are neglected.

The conservation equations for the fluid are the incompressible Stokes equations:

$$\partial_i v_i = 0, \tag{2.3}$$

$$-\partial_i p + \eta \partial_j^2 v_i = 0, \tag{2.4}$$

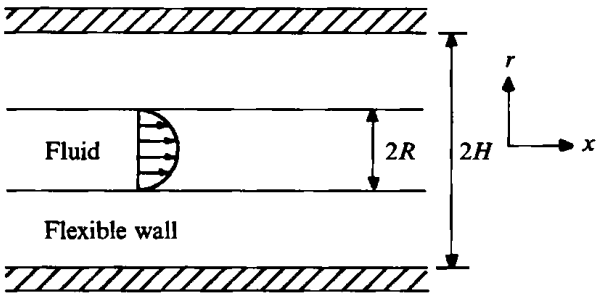


FIGURE 1. Configuration and definition of coordinate systems.

where $v_i$ is the fluid velocity, $p$ is the pressure and $\partial_i = (\partial/\partial x_i)$. The stress in the fluid is

$$\tau_{ij} = -p\delta_{ij} + \eta(\partial_i v_j + \partial_j v_i). \tag{2.5}$$

The boundary conditions in the fluid at the centre of the tube ($r = 0$) are the symmetry conditions $v_r = 0$ and $\partial_r v_x = 0$, while the boundary conditions at the interface between the fluid and the flexible medium are the continuity of velocity and stress, which are be discussed a little later.

The wall of the tube is considered to be incompressible and impermeable to the fluid, and the conservation equations are similar to those used earlier for polymer gels (Harden *et al.* 1991; Kumaran 1993). The dynamics of the medium is described by a displacement field $u_i$, which represents the displacement of the material points in the medium from their steady state positions due to the fluctuations in the stresses at the interface. The velocity field in the medium is $v_i = \partial_t u_i$, the time derivative of the displacement field. In an incompressible viscoelastic solid, the displacement field satisfies (Landau & Lifshitz 1989)

$$\partial_i u_i = 0 \tag{2.6}$$

while the momentum conservation condition is

$$-\partial_i p + G\partial_j^2 u_i + \eta_s \partial_j^2 v_i = 0. \tag{2.7}$$

Here, $p$ is the pressure, $\eta_s$ is the viscosity of the wall, $G$ is the shear modulus of elasticity and the bulk modulus is considered to be infinite since the medium is incompressible. The second term on the left side of the above equation is the divergence of an elastic stress due to the strain in the medium, while the third term on the left is the divergence of a viscous stress due to the strain rate. The expression for the stress tensor that has been used in deriving the above equation is

$$\sigma_{ij} = -p\delta_{ij} + (G + \eta_s \partial_t)(\partial_i u_j + \partial_j u_i), \tag{2.8}$$

where $\partial_t \equiv (\partial/\partial t)$. Note that $\sigma_{ij}$ is used for the stress in the wall, and $\tau_{ij}$ for the stress in the fluid. Since the flexible medium is fixed to a rigid surface at $r = HR$, the boundary condition at this surface is $u_i = 0$. In addition, the continuity of velocity and stress conditions at the interface $r = R$ are

$$v_i = \partial_t u_i, \quad \tau_{ij} = \sigma_{ij} - \delta_{in}\delta_{jn} T \partial_s^2 u_n, \tag{2.9}$$

where $T$ is the surface tension, $n$ is the normal direction (there is no summation over $n$), $u_n$ is the normal displacement and $\partial_s$ is the gradient along the tangential direction to the surface. In the present case, we consider surface displacements that are a

function of the axial coordinate only, and $\partial_s \equiv \partial_x$. The product $\delta_{in}\delta_{jn}$ ensures that the surface tension term contributes only to the stress normal to the surface, and not to any of the other normal or shear stresses.

It is convenient to scale the lengths in the problem by the radius of the tube $R$, and the times by $(\eta/G)$, the ratio of the viscosity of the fluid and the elasticity of the medium. The appropriate scale for the velocity and pressure then become $(GR/\eta)$ and $G$ respectively. With this non-dimensionalization, the mean fluid velocity (2.1) becomes

$$\bar{v} = \Gamma(1-r^2), \tag{2.10}$$

where $\Gamma = (V\eta/GR)$ is a dimensionless velocity. This is similar to the Weissenberg number for viscoelastic materials (Chen 1991; Su & Khomami 1992), with the difference that $\Gamma$ is expressed in terms of the viscosity of the fluid and the elasticity of the medium, while the Weissenberg number contains the ratio of the viscosity and elasticity of the same viscoelastic fluid. From this point onwards, all the dynamical variables will be expressed in dimensionless form.

In the stability analysis, the dynamical variables in the base state are perturbed by small axisymmetric disturbances of the form

$$v_i = \tilde{v}_i(r)\exp(\mathrm{i}kx+st), \quad u_i = \tilde{u}_i(r)\exp(\mathrm{i}kx+st), \tag{2.11}$$

where $k$ is the wavenumber and $s$ is the growth rate of the perturbations. Note that $k$ is real and $s$ is, in general, a complex growth rate since the temporal stability of the fluctuations is considered. The conservation equations for the fluid velocity disturbance, derived from (2.3) and (2.4), are

$$(\mathrm{d}_r + r^{-1})\tilde{v}_r + \mathrm{i}k\tilde{v}_x = 0, \tag{2.12}$$

$$-\mathrm{d}_r\tilde{p} + (\mathrm{d}_r^2 + r^{-1}\mathrm{d}_r - r^{-2} - k^2)\tilde{v}_r = 0, \tag{2.13}$$

$$-\mathrm{i}k\tilde{p} + (\mathrm{d}_r^2 + r^{-1}\mathrm{d}_r - k^2)\tilde{v}_x = 0, \tag{2.14}$$

where $\mathrm{d}_r$ is the total derivative $(\mathrm{d}/\mathrm{d}_r)$, since the eigenfunctions $\tilde{v}_r$, $\tilde{v}_x$ and $\tilde{p}$ are functions of $r$ only. Note that there is no coupling between the mean and fluctuating velocity in the conservation equations because the Stokes equations are linear. However, there is a coupling due to the boundary conditions, which will be considered shortly. The scaled equations for the perturbations to the displacement field in the wall, from (2.6) and (2.7), are

$$(\mathrm{d}_r + r^{-1})\tilde{u}_r + \mathrm{i}k\tilde{u}_x = 0, \tag{2.15}$$

$$-\mathrm{d}_r\tilde{p} + (\mathrm{d}_r^2 + r^{-1}\mathrm{d}_r - r^{-2} - k^2)(1+\eta_r s)\tilde{u}_r = 0, \tag{2.16}$$

$$-\mathrm{i}k\tilde{p} + (\mathrm{d}_r^2 + r^{-1}\mathrm{d}_r - k^2)(1+\eta_r s)\tilde{u}_x = 0, \tag{2.17}$$

where $\eta_r = (\eta_s/\eta)$ is the ratio of the viscosity of the wall and the fluid.

The boundary conditions for the velocity field at the interface $r = 1$ are

$$\tilde{v}_r = s\tilde{u}_r, \quad \tilde{v}_x - 2\Gamma\tilde{u}_r = s\tilde{u}_x. \tag{2.18}$$

The second term on the left side of the boundary condition for $\tilde{v}_x$ represents the variation in the velocity at the interface due to the gradient in the mean velocity in the fluid, and the factor $-2\Gamma$ in this term is $(\partial_r \bar{v})|_{r=1}$, the gradient in the mean velocity at the interface (see (2.10)). This is the only coupling between the mean velocity and the fluctuations, and is responsible for the instabilities that are discussed later on. Finally, we have the matching conditions for the shear and normal stresses at the surface:

$$\tilde{\tau}_{rr} = \tilde{\sigma}_{rr} + \Lambda k^2\tilde{u}_r, \quad \tilde{\tau}_{xr} = \tilde{\sigma}_{xr}, \tag{2.19}$$

where $A = (T/GR)$ is a capillary number that gives the ratio of the surface tension and the elastic stresses. There is no contribution due to the mean flow in the boundary condition for the shear stress, because the derivative of the shear stress is continuous across the interface in the mean flow from (2.1) and (2.2). The stresses in the wall and fluid are

$$\tilde{\tau}_{rr} = -\tilde{p} + 2\mathrm{d}_r \tilde{v}_r, \quad \tilde{\tau}_{xr} = \mathrm{d}_r \tilde{v}_x + \mathrm{i}k\tilde{v}_r, \tag{2.20}$$

$$\tilde{\sigma}_{rr} = -\tilde{p} + 2(1+\eta_r s)\,\mathrm{d}_r \tilde{u}_r, \quad \tilde{\sigma}_{xr} = (1+\eta_r s)(\mathrm{d}_r \tilde{u}_x + \mathrm{i}k\tilde{u}_r). \tag{2.21}$$

The conservation equations (2.12)–(2.17) and the boundary conditions (2.18) and (2.19), along with the symmetry conditions ($\tilde{v}_r = 0$ and $\mathrm{d}_r \tilde{v}_x = 0$) at $r = 0$ and the zero displacement conditions ($\tilde{u}_r = 0$ and $\tilde{u}_x = 0$) at $r = H$ can now be solved for the displacement fields and the growth rate.

The conservation equations for the fluid, (2.12)–(2.14), can easily be solved to obtain the following eigenfunctions for $\tilde{v}_r$ and $\tilde{v}_x$ (Happel & Brenner 1965):

$$\tilde{v}_r = A_1 r I_0(kr) + A_2 I_1(kr), \tag{2.22}$$

$$\tilde{v}_x = (\mathrm{i}A_1/k)[2I_0(kr) + krI_1(kr)] + \mathrm{i}A_2 I_0(kr), \tag{2.23}$$

$$\tilde{p} = 2A_1 I_0(kr), \tag{2.24}$$

where $I_0(kr)$ and $I_1(kr)$ are modified Bessel functions, and $A_1$ and $A_2$ are constants to be determined from the boundary conditions at the interface. The mass and momentum equations in the wall, (2.15)–(2.17), can be solved in a similar manner:

$$\tilde{u}_r = B_1 r K_0(kr) + B_2 K_1(kr) + B_3 r I_0(kr) + B_4 I_1(kr), \tag{2.25}$$

$$\tilde{u}_x = (\mathrm{i}B_1/k)[2K_0(kr) - krK_1(kr)] - \mathrm{i}B_2 K_0(kr) + (\mathrm{i}B_3/k)[2I_0(kr) + krI_1(kr)] + \mathrm{i}B_4 I_0(kr), \tag{2.26}$$

$$\tilde{p} = 2(1+\eta_r s)[B_1 K_0(kr) + B_3 I_0(kr)], \tag{2.27}$$

where $K_0(kr)$ and $K_1(kr)$ are also modified Bessel functions, and $B_1$, $B_2$, $B_3$ and $B_4$ are constants to be determined from the boundary conditions. Two of these are fixed by the zero displacement conditions ($\tilde{u}_r = 0$ and $\tilde{u}_x = 0$) at $r = H$, while the other two are determined from the conditions at the interface.

The solutions for the velocity and pressure fields, (2.22)–(2.27), can be inserted into the velocity and stress conditions at the interface, (2.18) and (2.19), and the zero displacement condition $\tilde{u}_i = 0$ at $r = H$, to obtain the characteristic matrix of the form:

$$\boldsymbol{M} \cdot \boldsymbol{C}^T = 0, \tag{2.28}$$

where $\boldsymbol{A}$ is the matrix of the amplitudes:

$$\boldsymbol{C} = [A_1, A_2, B_1, B_2, B_3, B_4], \tag{2.29}$$

and $\boldsymbol{M}$ is a $6 \times 6$ matrix of coefficients, in which the six rows are obtained from the two velocity conditions at the interface (2.18), the two stress conditions at the interface (2.19) and the two zero displacement conditions at $r = H$. The characteristic equation is obtained by setting the determinant of the characteristic matrix $\boldsymbol{M}$ equal to zero. The solution of the characteristic equation gives the growth rate $s$ as a function of the wavenumber $k$ for different values of $H$, $\Gamma$ and $\eta_r$. The effect of changes in the parameter values on the growth rate of the fluctuations is analysed in the next section.

Though the present analysis is a temporal stability analysis, it is possible to obtain some information about the spatial stability of perturbations in the initial value analysis. The spatial and temporal modes are identical for neutrally stable perturbations, because both the spatial and temporal growth rates are imaginary in this case. Therefore, the stability boundaries for the initial value problem are identical to those calculated here. In addition, the group velocity of the most unstable waves in the spatial stability analysis can also be determined from a knowledge of the temporal growth rate from the relation (Drazin & Reid 1981)

$$c_g = -\partial s_I/\partial k, \tag{2.30}$$

where $s_I$ is the imaginary part of the growth rate (frequency) and $k$ is the wavenumber. Some results for the group velocity are also presented in the next section.

## 3. Results

The characteristic equation turns out to be a quadratic equation which has two roots. The characteristic equation was determined analytically, and the two roots of the equation were obtained using symbolic computation. However, the algebra required for determining the equation is tedious and the roots are complicated, so we do not give the details of the calculation here. In this section, we report the scaling behaviour of the critical velocity, wavenumber and frequency of the most unstable mode in different limits; these are summarized in tables 1–3. Owing to the complexity of the algebra involved, it was not possible to obtain the asymptotic results analytically, and the limiting behaviour was obtained by fitting scaling relations for the critical velocity, wavenumber and frequency. The accuracy of the scaling relations are compared with the analytically determined values in figures 10–13, which are available on request from the authors or from the editorial offices of the journal. The empirical relations could prove convenient for comparing the theory with experimental results.

The two solutions for the complex growth rate $s$ are functions of four dimensionless parameters: the mean velocity $\Gamma$, the ratio of the viscosities of the wall and the fluid $\eta_r = (\eta_s/\eta)$, the ratio of radii $H$ and the capillary number $\Lambda$. Here, the behaviour of the growth rate is analysed for a range of parameter values of $H$, $\eta_r$ and $\Lambda$, and the results are organized as follows. In §3.1, the case $\eta_r = 0$, $\Lambda = 0$ and $H$ varying is considered, and some qualitative features of the unstable mode are discussed. Then the effect of variation in the capillary number $\Lambda$ at $\eta_r = 0$ and the effect of variation in $\eta_r$ at $\Lambda = 0$ are examined in §§3.2 and 3.3 respectively.

### 3.1. *Case 1:* $\eta_r = 0$, $\Lambda = 0$

In this subsection, we consider a system in which the viscosity of the wall is zero, and there is no surface tension. This is the most unstable situation, because an increase in surface tension stabilizes the interface and an increase in viscosity stabilizes the fluctuations due to increased viscous dissipation. Therefore, this system is analysed in some detail.

In the absence of flow ($\Gamma = 0$), the roots of the characteristic equation are always real and negative, indicating that the system is stable. As the fluid velocity is increased, however, one of the roots becomes positive beyond a transition value $\Gamma > \Gamma_t$. This is illustrated in figure 2(*a*), where the real parts of the two solutions for the growth rate, $s_{R1}$ and $s_{R2}$, are shown as a function of $k$. One of the roots, $s_{R2}$, is always negative, while the other root, $s_{R1}$, becomes positive for $\Gamma > \Gamma_t$, where $\Gamma_t$ is a function of the wavenumber. The magnitude of the unstable root $s_{R1}$ decreases to zero in the limit

| Limit | $\Gamma_c$ | $k_c$ | $-s_{Ic}$ |
|---|---|---|---|
| $H-1 \ll 1$, $\Lambda = 0$ | 4.109 | $1.515(H-1)^{-1}$ | 1.827 |
| $H-1 \ll 1$, $\Lambda \gg 1$ | $1.163\Lambda^{0.75}(H-1)^{-0.75}$ | $1.665\Lambda^{-0.25}(H-1)^{-0.75}$ | $1.180\Lambda^{0.5}(H-1)^{-0.5}$ |
| $H \gg 1$, $\Lambda \ll 1$ | 0.7685 | 0.6789 | 0.4104 |
| $H \gg 1$, $\Lambda \gg 1$ | $0.335\Lambda^{0.4}$ | $1.125\Lambda^{-0.4}$ | 0.369 |

TABLE 1. The power law dependence of $\Gamma_c$, $k_c$ and $-s_{Ic}$ on $\Lambda$ for $\eta_r = 0$

| | |
|---|---|
| $(\eta_r - 1) \ll 1$ | $H_{min} = 2.115(\eta_r - 1)^{0.25}$ |
| $\eta_r \gg 1$ | $H_{min} = \exp(1.011 + 0.0832\eta_r^2)$ |

TABLE 2. The empirical relations for $H_{min}$ for $\Lambda = 0$ in the limits $(\eta_r - 1) \ll 0$ and $\eta_r \gg 0$

| Limit | $\Gamma_c$ | $k_c$ | $-s_{Ic}$ |
|---|---|---|---|
| $H-1 \ll 1$, $\eta_r \ll 1$ | 4.109 | $\dfrac{1.515}{H-1}$ | 1.8270 |
| $H-1 \ll 1$, $1-\eta_r \ll 1$ | $3.752(1-\eta_r)^{-1.50}$ | $\dfrac{1.91(-\log(1-\eta_r))^{0.6}}{H-1}$ | $1.227(1-\eta_r)^{-0.5}$ |
| $H \gg 1$, $\eta_r \ll 1$ | 0.7685 | 0.6789 | 0.4104 |
| $H \gg 1$, $\eta_r \gg 1$ | $\exp(-0.01188 + 0.08333\eta_r^2)$ | $0.4083/\Gamma_c$ | 0.4082 |

TABLE 3. The empirical relations for $\Gamma_c$, $k_c$ and $-s_{Ic}$ for $\Lambda = 0$ and $(1-\eta_r) \ll 1$ and $\eta_r \ll 1$

$k \to 0$, while the magnitude of the stable root $s_{R2}$ diverges proportional to $k^{-2}$. In the limit $k \gg 1$, both $s_{R1}$ and $s_{R2}$ converge towards a value of $-1$. The imaginary parts of the two roots, $s_{I1}$ and $s_{I2} = -s_{I1}$, are shown in figure 2(*b*). From this, it can be seen that the unstable root has a negative imaginary part, indicating that the waves which become unstable travel downstream, while the upstream travelling waves are always stable. Further calculations indicate that the unstable mode is a downstream travelling wave for all values of $\eta_r$ and $\Lambda$, while the upstream travelling wave is always stable.

The transition velocity, $\Gamma_t$, shown in figure 3, increases $\propto k^{-2}$ in the limit $k \ll 1$, and increases $\propto k^2$ in the limit $k \gg 1$ for all values of $H$. The minimum value of the transition velocity, which is the velocity at which an instability is first observed, occurs at finite wavenumber. For $k \gg 1$, the value of $\Gamma_t$ approaches a limiting behaviour which is independent of $H$ because the behaviour of short-wavelength fluctuations is insensitive to the thickness of the wall. For $k \ll 1$, it is observed that the transition velocity increases as the thickness of the wall $H$ decreases.

The critical velocity for the flow is the minimum velocity at which unstable perturbations can exist, and is the minimum of the $\Gamma_t$, $k$ curves. Figure 4(*a*) shows that $\Gamma_c$ decreases from 4.109 in the limit $(H-1) \ll 1$ to 0.7685 in the limit $H \gg 1$. This

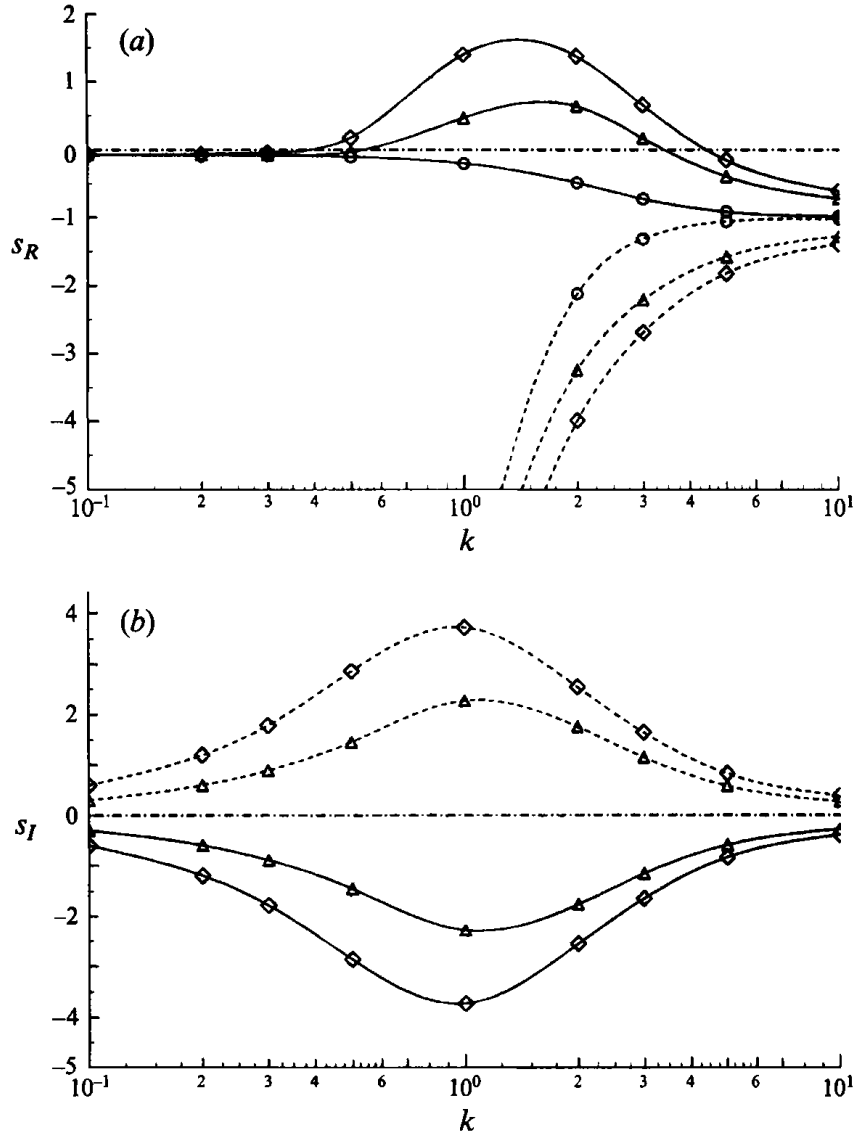


FIGURE 2. (*a*) The real part of the growth rate $s_R$, and (*b*) the imaginary part $s_I$ as a function of $k$ for $\eta_r = 0$, $\Lambda = 0$ and $H = 2$. The solid line represents the first root $s_1$ and the broken line represents the second root $s_2$: —○—, $\Gamma = 0$; —△—, $\Gamma = 5$; —◇—, $\Gamma = 10$.

indicates that in the absence of surface tension and viscosity of the flexible medium, an instability could be induced for all values of $H$ at sufficiently high velocity. It might seem surprising that $\Gamma_c$ remains finite for $(H-1) \ll 1$, but it should be noted that we are only considering fluctuations whose amplitude is small compared to the thickness of the surface even in the limit $(H-1) \ll 1$. The wavenumber $k_c$, frequency $s_c$ and the group velocity $c_g$ of the most unstable mode are shown in figures 4(*b*)–(*d*) respectively. It is interesting to note that the group velocity is negative for $H < 2$, becomes zero at $H = 2$ and then increases and assumes a constant value for $H \gg 1$. This implies that the most unstable mode in the spatial stability problem would move upstream for small $H$ and downstream for large $H$. The power law behaviour of $\Gamma_c$, the wavenumber of the most unstable mode $k_c$, and the frequency of the most unstable mode $s_{Ic}$ in the limits $(H-1) \ll 1$ and $H \gg 1$ are given in table 1.

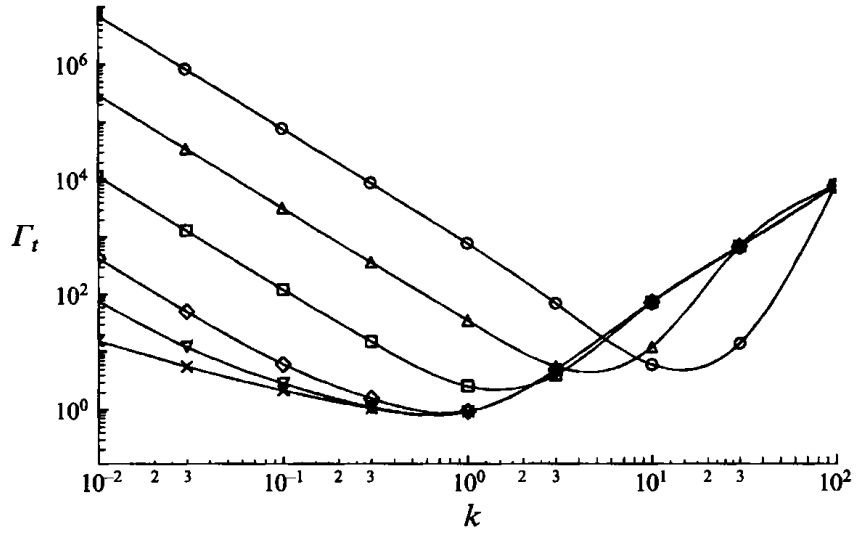


FIGURE 3. The transition velocity, $\Gamma_t$ as a function of wavenumber $k$ for different values of the ratio of radii $H$ and for $\eta_r = 0$ and $\Lambda = 0$: —○—, $H = 1.1$; —△—, $H = 1.3$; —□—, $H = 2.0$; —◇—, $H = 5$; —▽—, $H = 10$; —×—, $H = 100$.

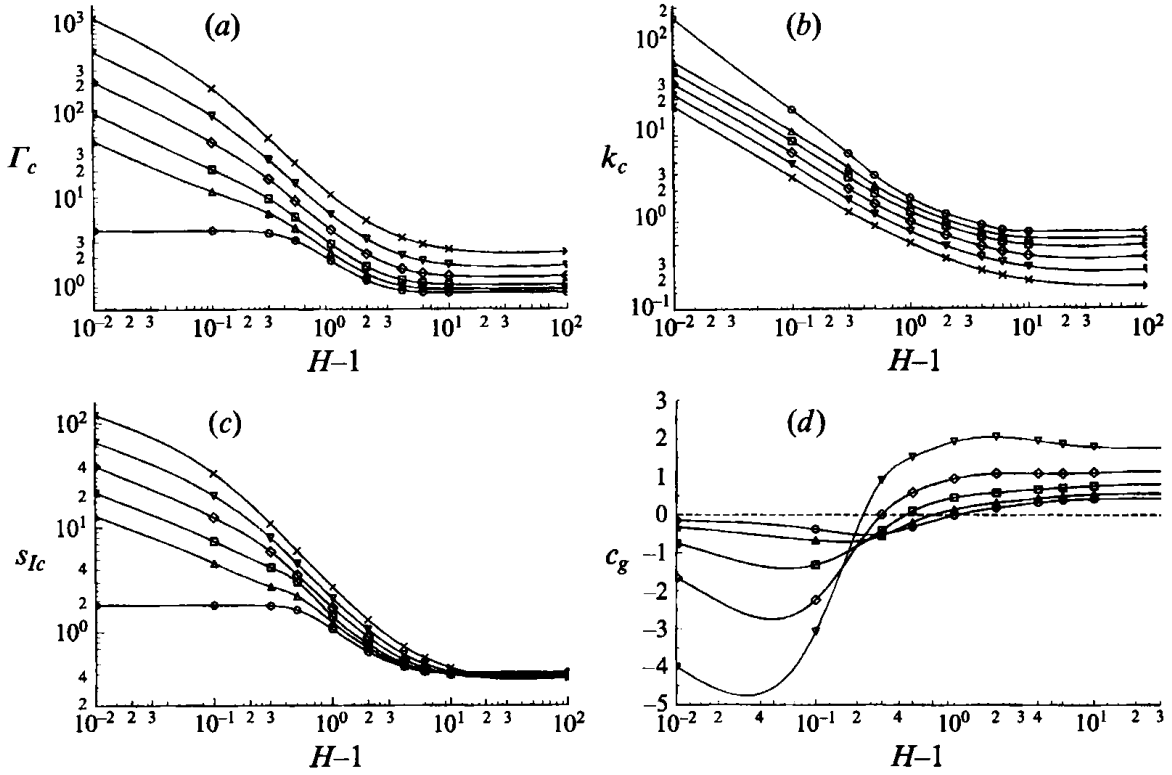


FIGURE 4. (*a*) The critical velocity $\Gamma_c$, (*b*) the wavenumber of the most unstable mode $k_c$, (*c*) the frequency of the most unstable mode $-s_{Ic}$ and (*d*) the group velocity $c_g$ as a function of $(H-1)$ for $\eta_r = 0$ and different values of $\Lambda$: —○—, $\Lambda = 0$; —△—, $\Lambda = 1$; —□—, $\Lambda = 3$; —◇—, $\Lambda = 10$; —▽—, $\Lambda = 30$; —×—, $\Lambda = 100$.

### 3.2. *Case 2:* $\eta_r = 0$, $\Lambda \neq 0$

An increase in the surface tension does not change the qualitative behaviour of the transition velocity, but it stabilizes the short-wavelength fluctuations. This is illustrated in figure 5, where the transition velocity $\Gamma_t$ is shown as a function of $k$ for $H = 2$ and

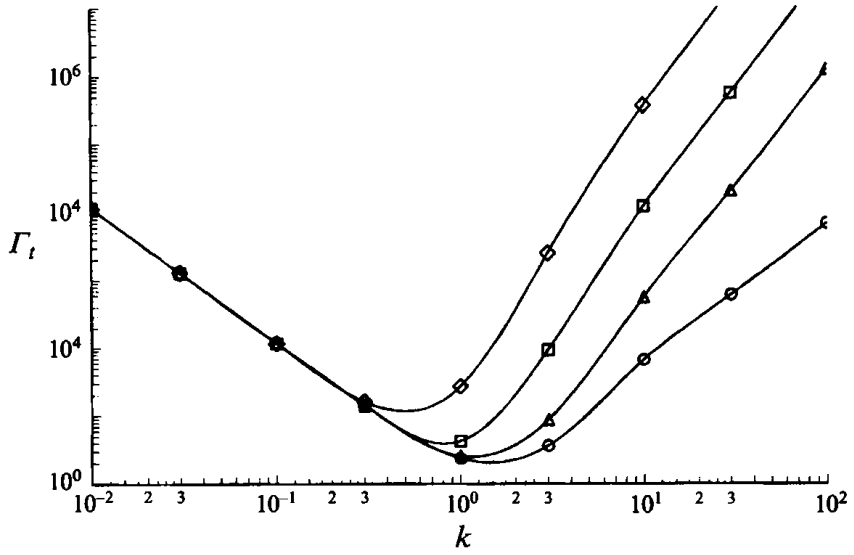


FIGURE 5. The transition velocity, $\Gamma_t$, as a function of the wavenumber $k$ for $H = 2$, $\eta_r = 0$ and for different values of the capillary number $\Lambda$: —○—, $\Lambda = 0$; —△—, $\Lambda = 1.0$; —□—, $\Lambda = 10$; —◇—, $\Lambda = 100$.

different values of $\Lambda$. As might be expected, there is no change in the transition velocity in the limit $k \ll 1$ because the stress due to the surface tension is proportional to $k^2$ in this limit. However, the surface tension has a significant effect in the limit $k \gg 1$, and $\Gamma_t$ increases $\propto k^{3.5}$ in this limit (in contrast to the increase $\propto k^2$ for $\Lambda = 0$).

The critical velocity, $\Gamma_c$, is shown as a function of $(H-1)$ for different values of $\Lambda$ in figure 4(*a*). This has a finite value for $H \gg 1$, but the presence of surface tension changes the qualitative behaviour in the limit $(H-1) \ll 1$, where we find that $\Gamma_c$ increases $\propto (H-1)^{-0.75}$ (in contrast to the finite value of $\Gamma_c$ in this limit in the absence of surface tension). There is also a change in the power law behaviour of $k_c$, and $-s_{Ic}$ (figures 4*b*, *c*) which are given in table 1.

The empirical relations given in table 1 for the regime $\Lambda \gg 1$ and $(H-1) \ll 1$ turn out to be quite accurate for $\Lambda > 0.1$, though there is a little discrepancy for $0.01 < \Lambda < 0.1$. The empirical relations for $\Lambda \gg 1$ and $H \gg 1$ are accurate only for $\Lambda > 10^4$. A comparison between the theoretical curves and the empirical relations is given in figures 10(*a–c*) and 11(*a–c*) which are available from the author or from the editorial office of the Journal.

### 3.3. *Case 3:* $\Lambda = 0$, $\eta_r \neq 0$

A variation in the ratio of viscosities, $\eta_r$, changes the qualitative behaviour of the transition velocity $\Gamma_t$. The transition velocity is shown as a function of $k$ for different values of $H$ for $\eta_r = 0.3$ in figure 6(*a*), for $\eta_r = 1.0$ in figure 6(*b*) and for $\eta_r = 3.0$ in figure 6(*c*). From these figures, it can be seen that the transition velocity decreases as the wavenumber $k$ is increased, reaches a minimum and then increases again as $k$ is further increased. In addition, an increase in $\eta_r$ tends to increase the critical velocity owing to the increased viscous dissipation in the wall.

Further, figures 6(*a–c*) reveal a rather complex dependence of the transition velocity on $H$ and $k$ which is very different from the case $\eta_r = 0$. In particular, the following features can be observed:

(i) From figures 6(*a*, *b*), it can be seen that the transition velocity $\Gamma_t$ decreases as $k$ is decreased from $\infty$, and then it increases and diverges at a minimum value $k = k_{min}$. This is a common feature of the transition velocity curve for $\eta_r \leqslant 1$, and $k_{min}$ can be

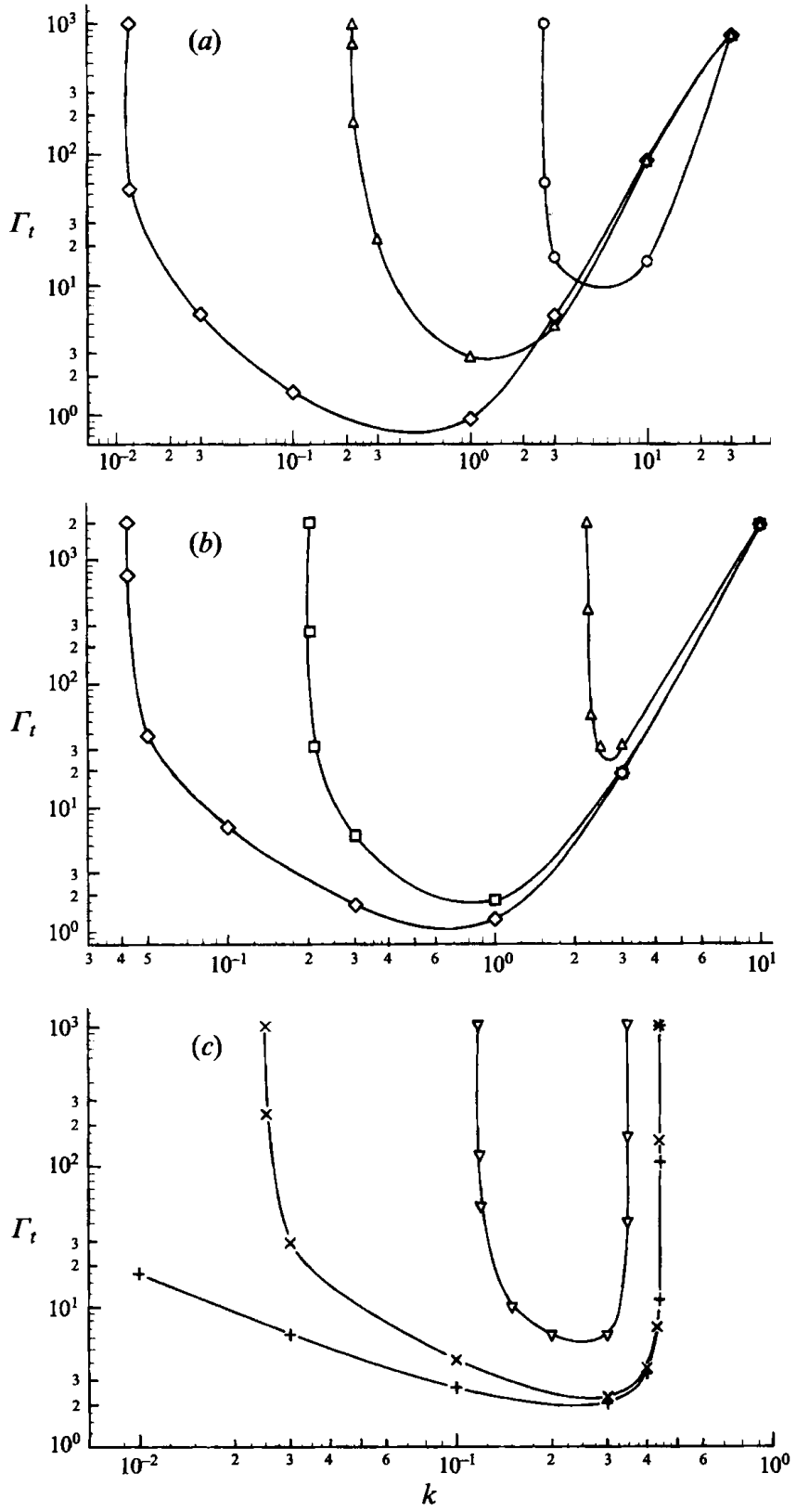


FIGURE 6. The transition velocity $\Gamma_t$ as a function of the wavenumber $k$ for $\Lambda = 0$ and (*a*) $\eta_r = 0.3$; (*b*) $\eta_r = 1$; and (*c*) $\eta_r = 3$. —○—, $H = 1.3$; —△—, $H = 2.0$; —□—, $H = 3.0$; —◇—, $H = 5.0$; —▽—, $H = 7.0$; —×—, $H = 11.0$; —+—, $H = 101.0$.

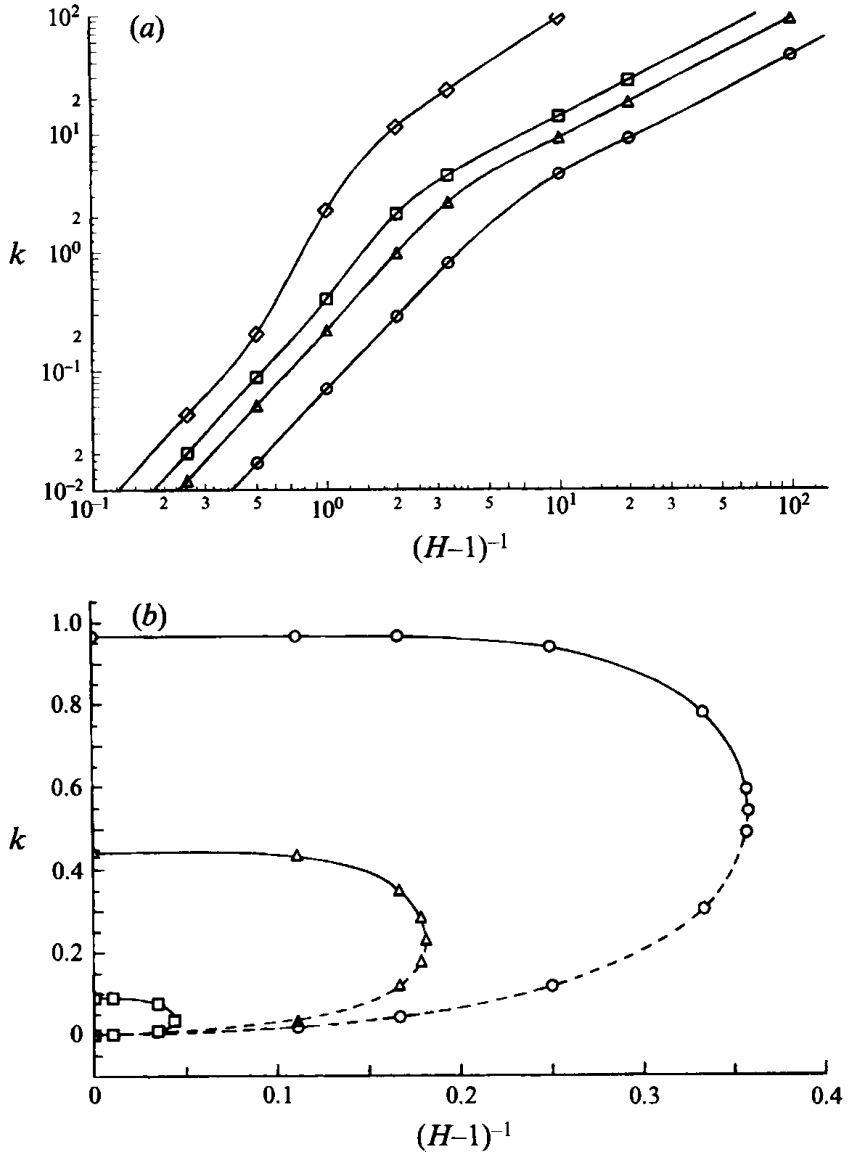


FIGURE 7. (*a*) The minimum wavenumber $k_{min}$ for the existence of unstable modes as a function of $(H-1)^{-1}$ for $A = 0$ and for different values of $\eta_r$: —○—, $\eta_r = 0.1$; —△—, $\eta_r = 0.3$; —□—, $\eta_r = 0.5$; —◇—, $\eta_r = 1$. (*b*) As (*a*) but for the minimum wavenumber $k_{min}$ (broken line) and the maximum wave number $k_{max}$ (solid line): —○—, $\eta_r = 2.0$; —△—, $\eta_r = 3.0$; —□—, $\eta_r = 5.0$.

obtained analytically by solving the characteristic equation for $\Gamma = \infty$. The minimum wavenumber is shown as a function of $(H-1)^{-1}$ for different values of $\eta_r$ in figure 7(*a*). This figure shows that $k_{min}$ increases $\propto (H-1)^{-1}$ for $(H-1) \ll 1$, while $k_{min}$ decreases $\propto H^{-2.5}$ for $H \gg 1$.

(ii) Figure 6(*c*) shows that for $\eta_r = 3.0$, the transition velocity $\Gamma_t$ diverges both at a maximum wavenumber $k_{max}$ and a minimum wavenumber $k_{min}$, and decreases to a minimum value at an intermediate value of $k$. Figure 7(*b*) shows $k_{max}$ and $k_{min}$ as a function of $(H-1)^{-1}$ for different values of $\eta_r$. In the limit $H \gg 1$, an increase in $\eta_r$ tends to decrease $k_{max}$ but does not cause much variation in $k_{min}$. As $H$ is decreased, the difference $k_{max} - k_{min}$ decreases, until $k_{max} = k_{min}$ at a minimum value $H = H_{min}$. The equality of $k_{min}$ and $k_{max}$ has the following physical significance: for $H < H_{min}$, there are no unstable modes even in the limit $\Gamma \to \infty$, while for $H = H_{min}$ fluctuations with wavenumber $k = k_{min} = k_{max}$ become unstable in the limit $\Gamma \to \infty$. Thus, $H = H_{min}$

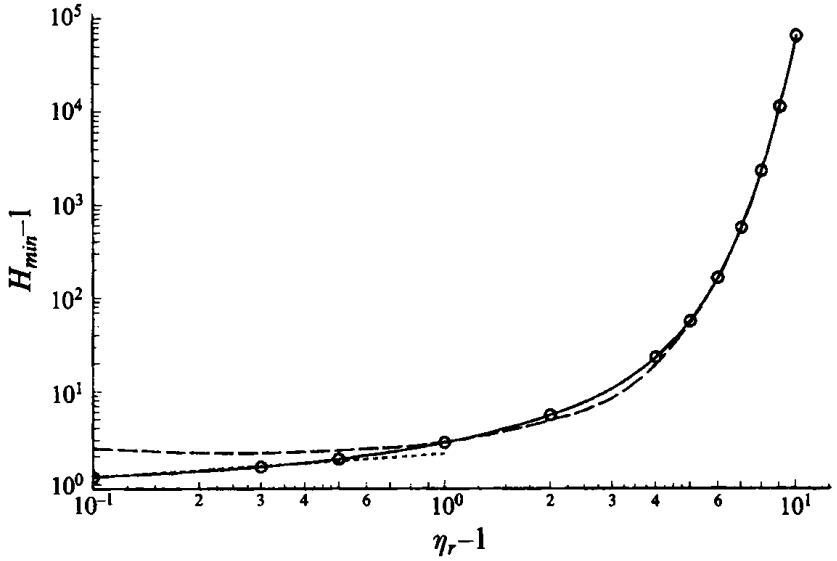


FIGURE 8. $(H_{min}-1)$ as a function of $(\eta_r-1)$ for $\Lambda = 0$, where $H_{min}$ is the minimum ratio of radii for the presence of unstable modes. The dotted line is the empirical relation in the limit $(\eta_r-1) \ll 1$ (table 2), while the broken line is the empirical relation in the limit $\eta_r \gg 1$ (table 2).

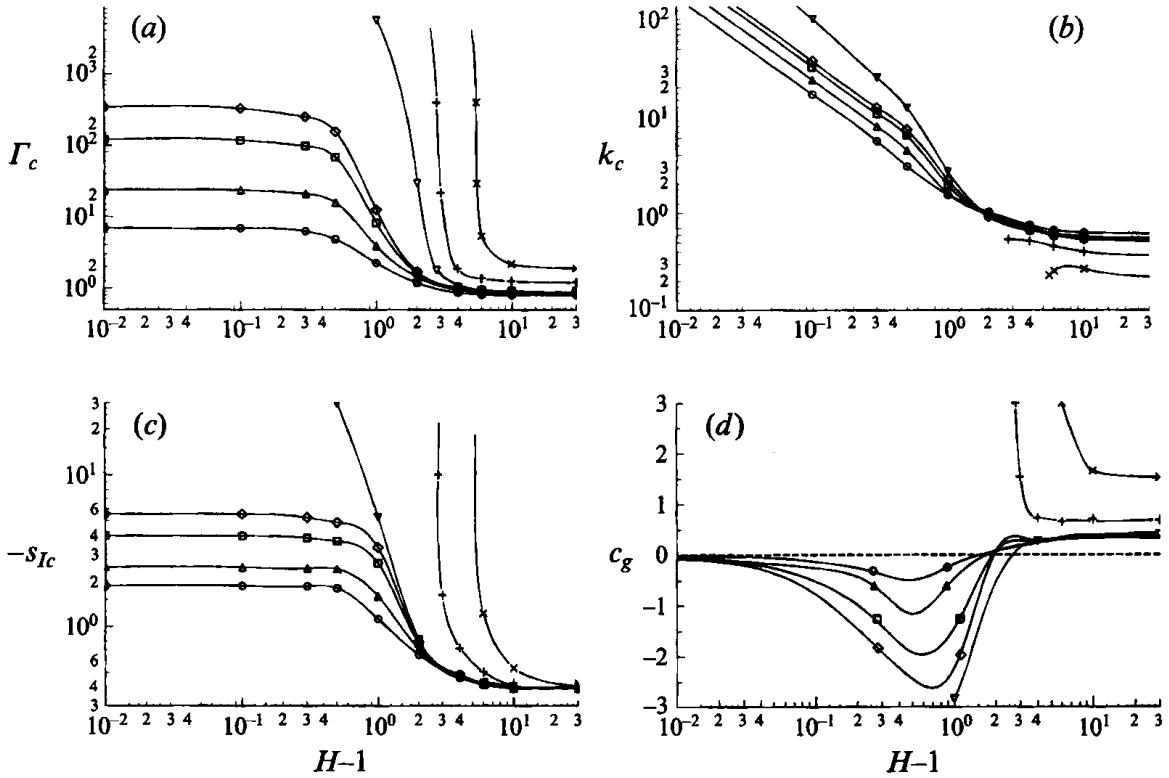


FIGURE 9. (*a*) The critical velocity $\Gamma_c$; (*b*) the wavenumber of the most unstable mode $k_c$; (*c*) the frequency of the most unstable mode $-s_{Ic}$; and (*d*) the group velocity $c_g$, as a function of $(H-1)$ for $\Lambda = 0$ and for different values of $\eta_r$: —○—, $\eta_r = 0.3$; —△—, $\eta_r = 0.7$; —□—, $\eta_r = 0.9$; —◇—, $\eta_r = 0.95$; —▽—, $\eta_r = 1.0$; —+—, $\eta_r = 2.0$; —×—, $\eta_r = 3.0$.

serves as a stability boundary in the $H$, $\eta_r$, $k$ parameter space for $\eta_r > 1$, and fluctuations are always stable for $H < H_{min}$ for a given value of $\eta_r$.

(iii) The minimum height $(H_{min}-1)$ is shown as a function of $(\eta_r-1)$ in figure 8. $(H_{min}-1)$ increases proportional to $(\eta_r-1)^{0.25}$ in the limit $(\eta_r-1) \ll 1$ (table 2), which

is shown by the dotted line in figure 8. In the limit $\eta_r \gg 1$, we find an exponential increase of the form $H_{min} = \exp(1.011 + 0.0832\eta_r^2)$ (table 2). This relation is shown by the broken line in figure 8, and it is fairly accurate for a variation of five orders of magnitude in $H_{min}$.

Having ascertained the unstable regions in the $k$, $H$, $\eta_r$, $\Lambda$ parameter space, the stability limits for $\eta_r > 0$ can be determined. Figure 9(*a*) shows $\Gamma_c$ as a function of $(H-1)$ for different values of $\eta_r$. For $\eta_r < 1$, $\Gamma_c$ decreases from one constant value in the limit $(H-1) \ll 1$ to another constant value for $H \gg 1$, while for $\eta_r > 1$ we find that $\Gamma_c$ diverges proportional to $(H-H_{min})^{-2}$ in the limit $H \to H_{min}$. The reason that $\eta_r = 1.0$ is a critical value regardless of the value of $H$ is due to the change in behaviour occurring at large $k$, for which the disturbance does not 'see' the thickness of the solid. The group velocity $c_g$ (figure 9*d*) has very different characteristics in the parameter regimes $\eta_r \leqslant 1$ and $\eta_r > 1$. For $\eta_r \leqslant 1$, the group velocity is qualitatively similar to the case $\eta_r = 0$, though its magnitude increases as $\eta_r$ increases. For $\eta_r > 1$, the group velocity diverges at $H = H_{min}$, and the neutrally stable modes always travel downstream. The empirical correlations for the wavenumber of the most unstable mode $k_c$ (figure 9*b*), and the frequency $-s_{Ic}$ (figure 9*c*) are given in table 3. A comparison between the theoretical values and the empirical relations is given in figure 12(*a–c*) for the limit $(H-1) \ll 1$ and in Figure 13(*a–c*) for the limit $H \gg 1$. These figures are available from the author or the editorial offices of the journal.

## 4. Conclusions

In this paper, the stability of the flow of a Newtonian fluid through a tube of radius $R$ surrounded by a flexible wall in the annular region of radius $R < r < HR$ was studied at low Reynolds number. The incompressible Stokes equations were used for the fluid, while the wall was modelled as an incompressible viscoelastic solid in which the stress has an elastic part proportional to the strain, and a viscous component proportional to the strain rate. The inertial terms were neglected in the conservation equations for both the fluid and the surface. The mean flow in the fluid is a parabolic Hagen–Poiseuille flow, while the wall is at rest in the base state. Small perturbations in the form of Fourier modes periodic in the axial direction were placed on the fluid velocity field and the strain field in the solid, and the stability of the flow to these fluctuations was determined using a linear stability analysis.

The conservation equations were solved analytically, and the characteristic equation for the growth rate was determined using the continuity of velocity and stress conditions at the interface. There are four dimensionless parameters that determine the stability of the system: the ratio of radii $H$, the dimensionless velocity $\Gamma = (V\eta/GR)$, the dimensionless capillary number $\Lambda = (T/GR)$ and the ratio of the surface and fluid viscosities $\eta_r = (\eta_s/\eta)$. Since the characteristic equation was obtained analytically, it was possible to obtain a fairly comprehensive picture of the stability behaviour over many magnitudes of variation in $\Lambda$, $H$ and $\eta_r$.

The mechanism leading to an instability in the present case is very different from that for the flow through a rigid tube. In a rigid tube, the fluid inertia is necessary for producing unstable perturbations since the conservation equations are not explicitly time dependent in the absence of inertia. However, in the present case there are unstable modes in the absence of inertia, and the time dependence enters through the elastic terms in the momentum conservation equation for the wall. The destabilizing mechanism is also different from that in the concentric flow of non-Newtonian fluids (Chen 1991; Su & Khomami 1992), where the instability is due to a normal stress

difference across the surface in the base state. In the present situation, there is a discontinuity in the strain rate at the surface because the viscous stress in the fluid is balanced by the elastic stress in the solid. This discontinuity results in an additional term in the boundary condition for the tangential velocity, proportional to the product of the mean fluid strain rate and the normal displacement of the surface, which gives the variation in the mean velocity due to the surface displacement. This is the only coupling between the mean flow and the fluctuations, and is responsible for destabilizing the fluctuations when the fluid velocity exceeds a critical value.

The physical reason for this instability can be better understood from the energy balance equation for the fluctuating component of the velocity. The energy balance equation can be written as (Chandrasekhar 1981):

$$\mathrm{d}_t E = C + S - D. \tag{4.1}$$

Here, $E$ is the total energy of the system, $D$ is the rate of viscous dissipation of energy due to the shear in the fluid and the wall, $C$ is the rate of transport of energy from the mean flow to the fluctuations due to the convective terms (Reynolds stress terms) in the momentum equation and $S$ is the deformation work due to the shear at the boundaries of the fluid and the wall. The deformation work is given by

$$S = \int_A \mathrm{d}A_i \tau_{ij} v_j, \tag{4.2}$$

where $\mathrm{d}A_i$ is an area element directed along the outward normal to the surface. The dissipation of energy in (4.1) has a stabilizing effect on the flow, while the other two terms could have a stabilizing or destabilizing effect. In a rigid tube, the deformation work $S$ is zero because the fluid velocity is zero at the wall, and the instability is caused by the transport of energy due to the Reynolds stresses $C$. In the present case, however, the convective terms have been neglected and it is the deformation work $S$ that has a destabilizing effect. A closer examination of this term reveals that the work done at the outer surface of the flexible surface is zero, because the velocity is zero at this surface. At the interface between the fluid and the flexible surface, the work done on the fluid is given by

$$S_f = \int_A \mathrm{d}A \tau_{rx} v_{xf}, \tag{4.3}$$

where $v_{xf}$ is the velocity fluctuation in the fluid. The deformation work done on the wall is

$$S_e = -\int_A \mathrm{d}A \sigma_{rx} v_{xe}. \tag{4.4}$$

There is a negative sign in the above expression because the outward normal is directed in the $-r$-direction. In situations where the shear stress and the tangential velocity are continuous across the interface, $S_f = -S_e$, indicating that there is a transfer of energy between the fluctuations in the fluid and wall, but no net transport of energy from the mean flow. In the present case, however, the shear stress is continuous across the interface from (2.19), but there is a discontinuity in the tangential velocity (2.18) which is proportional to $v_{xf} - v_{xe} = 2\Gamma u_r$. As was pointed out earlier, this additional term in the tangential velocity boundary condition is the only coupling between the mean flow and the fluctuations. Owing to this, the sum $(S_f + S_e)$ is non-zero, indicating that there is a net transport of energy from the mean flow to the fluctuations. This is facilitated

by the flexibility of the wall, and is responsible for destabilizing the flow when the fluid velocity increases beyond a transition value.

The destabilizing effect of the surface elasticity can be better illustrated for the simplified case of the plane interface between an infinite fluid and an infinite flexible medium, where $A = 0$ (no surface tension) and $\eta_r = 0$ (viscosity of the surface is zero). Here, it is sufficient to consider just the tangential velocity and the shear stress boundary conditions. In the absence of fluid flow ($\Gamma = 0$), the growth rate of the fluctuations is given by $s = (\tilde{v}_x/\tilde{u}_x)$ from the boundary condition for the velocity (2.18). The shear stress balance (2.19) indicates that the strain rate $\partial_r \tilde{v}_x$ in the fluid and the strain $\partial_r \tilde{u}_x$ in the flexible medium are of the same sign. Since the velocity in the fluid decays for $z \to \infty$ and the strain in the flexible medium decays for $z \to -\infty$, the stress balance condition implies that $\tilde{v}_x$ and $\tilde{u}_x$ are of opposite signs, and the real part of $s$ is negative. When there is a fluid flow, however, the growth rate is given by $s = (\tilde{v}_x - 2\Gamma\tilde{u}_r)/\tilde{u}_x$. The real part of the additional term $(-2\Gamma\tilde{u}_r/\tilde{u}_x)$ turns out to be positive for downstream travelling waves, and the real part of $s$ becomes positive when $\Gamma$ is increased beyond a critical value. Therefore, the presence of the coupling between the mean flow and fluctuations in the tangential velocity boundary condition is responsible for destabilizing the system when the velocity is increased beyond a critical value.

The characteristic equation for the growth rate is a quadratic equation, and there are two travelling wave solutions, one propagating downstream and the other upstream. In all the parameter regimes studied here, it is found that the downstream travelling wave becomes unstable, while the upstream travelling wave is stabilized as the fluid velocity is increased. In the absence of surface tension ($A = 0$) and viscosity of the surface ($\eta_r = 0$), the transition velocity at a given value of $H$ increases proportional to $k^2$ in the limit $k \gg 1$, and proportional to $k^{-2}$ in the limit $k \ll 1$. The mode with the lowest transition velocity has a finite wavenumber, and the transition velocity and wavenumber tend to increase as the thickness of the wall $(H-1)$ is decreased. The critical velocity, $\Gamma_c$, which is the minimum value of $\Gamma_t$, is finite in the limits $(H-1) \ll 1$ and $H \gg 1$. The group velocity of the most unstable mode in the spatial stability analysis, which can be determined from the present analysis using (2.30), shows an unusual behaviour. For $(H-1) \ll 1$, we find that the group velocity is negative and it decreases $\propto (H-1)^{-1}$, indicating that the most unstable waves travel upstream. As $H$ is increased, the group velocity increases and crosses zero at a finite value of $H$ and then reaches a constant value for $H \gg 1$, implying that the most unstable waves travel downstream for large $H$.

An increase in the surface tension tends to change the behaviour of short-wavelength modes, but the behaviour of long-wavelength modes remains unchanged, because the interfacial tension decreases proportional to $k^2$ in this limit. In the limit $k \gg 0$ the transition velocity increases proportional to $k^{3.5}$ (instead of the $k^2$ increase in the absence of surface tension). Other than this, the qualitative features of the $\Gamma_t$ *vs.* $k$ curves remain unchanged.

There is a qualitative change in the $\Gamma_t$ *vs.* $k$ curves when the ratio of viscosities $\eta_r$ is non-zero. For $\eta_r \leqslant 1$, only perturbations with wavenumber greater than a minimum value $k > k_{min}$ become unstable when the fluid velocity is increased beyond a transition value $\Gamma_t$, while perturbations with wavenumber $k < k_{min}$ remain stable even in the limit $\Gamma \to \infty$. For $\eta_r > 1$, only perturbations with an intermediate wavenumber $k_{min} < k < k_{max}$ become unstable when the velocity is increased beyond a transition value $\Gamma_t$, while perturbations with wavenumber $k < k_{min}$ or $k > k_{max}$ remain stable even for $\Gamma \to \infty$. As $H$ is decreased, $k_{min}$ increases and $k_{max}$ decreases so that there is a decrease in the range of wavenumbers that are potentially unstable. At a minimum value of

$H = H_{min}$ we find that $k_{min} = k_{max}$ and for $H < H_{min}$ all wavenumbers are stable even for $\Gamma \to \infty$. The minimum value $H_{min}$ for the presence of unstable modes was calculated over a range of values of $\eta_r$, and it was found that $H_{min}$ increases as $\eta_r$ is increased, and shows a strong divergence $\propto \exp(0.0832\eta_r^2)$ for large $\eta_r$. Empirical relations were developed for $H_{min}$, the critical velocity, and the wavenumber in the limit $(1-\eta_r) \ll 1$ and $\eta_r \gg 1$ (tables 2 and 3).

From the above discussion, it can be seen that the stability characteristics of the system are rather complex for $\eta_r > 0$. An interesting feature is that for $\eta_r < 1$, waves with wavenumber greater than a minimum value become unstable, while perturbations with wavenumber less than the minimum value are always stable. The behaviour for $\eta_r > 1$ is more unusual: it is found that perturbations with wavenumber in between a minimum and maximum value become unstable, while perturbations with wavenumber outside this range remain stable at all velocities. The range of potentially unstable wavenumbers decreases as the ratio of radii $H$ is decreased, until at $H = H_{min}$ the minimum and maximum wavenumbers coincide and all wavenumbers are stable. This complex behaviour would not have been obtained from simpler models, which approximate the wall dynamics by a spring term proportional to the normal displacement and a damping term proportional to the normal velocity (Carpenter & Garrad 1985, 1986), and it appears to be necessary to include a realistic description of the wall dynamics in order to accurately capture the stability characteristics. Further, this type of behaviour could not have been determined using the simpler continuation technique which involves a long-wavelength asymptotic analysis in the limit $k \to 0$ and analytic continuation for finite wavenumbers, because for $\eta_r > 0$, the perturbations are unstable only for $k > k_{min}$ and are stable in the limit $k \to 0$. This limitation has been overcome in the present case by obtaining an analytical solution for the velocity and strain fields and the growth rate.

The above analysis indicates that an instability could exist even in the absence of fluid inertia, and the mechanism suggested here is the transport of energy from the mean flow to the fluctuations due to deformation work done by the mean flow at the surface. As anticipated by Krindel & Silberberg (1979), we find that wall oscillations could be induced when the fluid velocity increases beyond a critical value. In their experimental analysis, Krindel & Silberberg considered the regime $H \gg 1$ (typically $10 < H < 30$), and the correlation obtained for the critical velocity was $\Gamma_c \propto H^{-1}$ in this limit. A direct comparison of the correlation with the results of this analysis is not possible because they do not report the value of the viscosity of the gel $\eta_s$. However, the present results do not appear to be in agreement with this correlation because we find that the critical velocity decreases to a finite value for $H \gg 1$. This disagreement could be due to the modification of the present instability due to inertial effects when the Reynolds number is not small. In addition, it must be noted that Krindel & Silberberg considered only two values of the ratio of radii $H$ in their experiments, and more experiments may be necessary to determine the exact dependence of the critical velocity on $H$. Further experiments with softer elastic materials and move viscous fluids would be able to probe the non-inertial limit. For example, if elastic materials with shear modulus in the range of $10\ \mathrm{N\,m^{-2}}$ and more viscous fluids with viscosity $0.1\ \mathrm{N\,s\,m^{-2}}$ are used, then inertial effects could be neglected if the tube radius is less than 1 mm in diameter, and it may be possible to observe the instability on a macroscopic scale.

## REFERENCES


BENJAMIN, T. B. 1960 Effect of a flexible boundary layer on hydrodynamic stability. *J. Fluid Mech.* **9**, 513.

BENJAMIN, T. B. 1963 The threefold classification of unstable disturbances in flexible surfaces bounding inviscid flows. *J. Fluid Mech.* **16**, 436.

BERTRAM, C. D. 1986 Unstable equilibrium behavior in collapsible tubes. *J. Biomech.* **19**, 61.

BERTRAM, C. D. 1987 The effects of wall thickness, axial strain and end proximity on the pressure area relation in collapsible tubes. *J. Biomech.* **20**, 863.

BERTRAM, C. D., RAYMOND, C. J. & PEDLEY, T. J. 1989 Mapping of instabilities during flow through collapsible tubes. *J. Fluids Structures* **4**, 125–154.

CANCELLI, C. & PEDLEY, T. J. 1985 A separated – flow model for collapsible-tube oscillations. *J. Fluid Mech.* **157**, 375.

CARPENTER, P. W. 1990 Status of transition delay using compliant walls. *Prog. Astro. Aero.* **123**, 79.

CARPENTER, P. W. & GAJJAR, J. S. G. 1990 A general theory for two and three dimensional wall-mode instabilities in boundary layers over isotropic and anisotropic compliant walls. *Theoret. Comput. Fluid Dyn.* **1**, 349.

CARPENTER, P. W. & GARRAD, A. D. 1985 The hydrodynamic stability of flows over Kramer-type compliant surfaces. Part 1. Tollmien–Schlichting instabilities. *J. Fluid Mech.* **155**, 465.

CARPENTER, P. W. & GARRAD, A. D. 1986 The hydrodynamic stability of flows over Kramer-type compliant surfaces. Part 2. Flow induced surface instabilities. *J. Fluid Mech.* **170**, 199.

CHANDRASEKHAR, S. 1981 *Hydrodynamic and Hydromagnetic Stability*. Dover.

CHEN, K. P. 1991 Interfacial instability due to the elastic stratification in concentric coextrusion of two viscoelastic fluids. *J. Non-Newtonian Fluid Mech.* **40**, 155.

DRAZIN, P. G. & REID, W. H. 1981 *Hydrodynamic Stability*. Cambridge University Press.

GREEN, C. H. & ELLEN, C. H. 1972 The stability of a plane Poiseuille flow between flexible walls. *J. Fluid Mech.* **51**, 403.

GUPTA, A. S. 1967 Stability of a visco-elastic film flowing down an inclined plane. *J. Fluid Mech.* **28**, 17.

HAPPEL, J. & BRENNER, H. 1965 *Low Reynolds Number Hydrodynamics*, Chap. 3. Prentice-Hall.

HARDEN, J. L., PLEINER, P. & PINCUS, P. A. 1991 Hydrodynamic modes on concentrated polymer solutions and gels. *J Chem. Phys.* **94**, 5208.

HOOPER, A. & BOYD, W. G. 1983 Shear flow instability at the interface between two viscous fluids. *J. Fluid Mech.* **128**, 507.

JENSEN, O. E. & PEDLEY, T. J. 1989 The existence of steady flow in a collapsed tube. *J. Fluid Mech.* **206**, 339.

KRAMER, M. O. 1957 Boundary-layer stabilization by distributed damping. *J. Aero. Sci.* **24**, 459.

KRAMER, M. O. 1960 Boundary layer stabilization by distributed damping. *J. Am. Soc. Naval Engrs* **74**, 25.

KRINDEL, P. & SILBERBERG, A. 1979 Flow through gel-walled tubes. *J. Colloid Interface Sci.* **71**, 34.

KUMARAN, V. 1993 Surface modes on a polymer gel of finite thickness. *J. Chem. Phys.* **98**, 3429.

KUMARAN, V., FREDRICKSON, G. H. & PINCUS, P. 1994 Flow induced instability at the interface between a fluid and a gel at low Reynolds number. *J. Phys. Paris* II **4**, 893–904.

LANDAHL, M. T. 1962 On the stability of a laminar incompressible boundary layer over flexible surface. *J. Fluid Mech.* **13**, 609.

LANDAU, L. D. & LIFSHITZ, E. M. 1989 *Theory of Elasticity*. Pergamon.

LIN, C. C. 1945*a* On the stability of two-dimensional parallel flows. Part 1. *Q. Appl. Maths* **3**, 117–142.

LIN, C. C. 1945*b* On the stability of two-dimensional parallel flows. Part 2. *Q. Appl. Maths* **3**, 218–234.

LIN, C. C. 1945*c* On the stability of two-dimensional parallel flows. Part 3. *Q. Appl. Maths* **3**, 277–301.

LIN, C. C. 1955 *The Theory of Hydrodynamic Stability*. Cambridge University Press.

RENARDY, Y. 1988 Stability of the interface in a two-layer Couette flow of upper convected Maxwell liquids. *J. Non-Newtonian Fluid Mech.* **28**, 99.

REYN, J. W. 1987 Multiple solutions and flow limitation for steady flow through a collapsible tube held by open ends. *J. Fluid Mech.* **174**, 467.

RILEY, J., GAD-EL-HAK, M. & METCALFE, R. W. 1988 Compliant coatings. *Ann. Rev. Fluid Mech.* **20**, 393.

SCHLICHTING, H. 1933 Zur Entstehung der Tubrulenz bei der Plattenstromung. *Z. Agnew. Math. Mech.* **13**, 171.

SHAQFEH, E. S. G., LARSON, R. G. & FREDRICKSON, G. H. 1989 The stability of gravity driven viscoelastic film-flow at low to moderate Reynolds number. *J. Non-Newtonian Fluid Mech.* **21**, 87.

SILBERBERG, A. 1987 Physico-chemical hydrodynamics in turbulent flows close to an interface. *Physico-chem. Hydrodyn.* **9**, 419.

SU, Y. Y. & KHOMAMI, B. 1992 Interfacial instability in multilayer viscoelastic fluids in slit and converging channel die geometries. *J. Rheol.* **36**, 357.

TOLLMIEN, W. 1929 Uber die Entstehung der Turbulenz. 1. *Mitt. Ges. Wiss. Gottingen, Math. Phys.* Klasse 21.

WATERS, N. D. & KEELY, A. M. 1987 The stability of two stratified non-Newtonian liquids in a Couette flow. *J. Non-Newtonian Fluid Mech.* **24**, 161.

YIH, C. S. 1970 Instability due to viscosity stratification. *J. Fluid Mech.* **27**, 337.